Computational Materials Science 198 (2021) 110684

Contents lists available at ScienceDirect

Computational Materials Science

journal homepage: www.elsevier.com/locate/commatsci

Lattice correspondence analysis on the formation mechanism for partial stacking faults in hexagonal close-packed metals

B. Li [a,*], Q. Sun [b], X.Y. Zhang [c,*]

[a] Department of Chemical and Materials Engineering, University of Nevada, Reno, NV 89557, USA
[b] Key Laboratory of Advanced Technologies of Materials (Ministry of Education), School of Material Science and Engineering, Southwest Jiaotong University, Chengdu 610031, China
[c] School of Materials Science and Engineering, Chongqing University, China

ARTICLE INFO

Keywords:
Stacking faults
Lattice correspondence
Twinning

ABSTRACT

Partial stacking faults (PSFs) have been frequently observed inside $\{10\bar{1}1\}$ and $\{10\bar{1}2\}$ twins in hexagonal close-packed (HCP) metals. Formation of PSFs, first described by Song and Gray, only displaces atoms on every other basal plane, in stark contrast to conventional SFs created by Shockley partial dislocations in which a global displacement vector can be defined. To experimentally verify this process is challenging. To understand the formation mechanism of the PSFs, in this work, we performed lattice correspondence analysis in atomistic simulations of $\{10\bar{1}1\}$ and $\{10\bar{1}2\}$ twinning modes in Mg, Ti and Co. In this strategy, the corresponding planes of the parent to the prismatic plane of the twin were pre-selected and tracked before and after twinning. Then, the atomic positions were examined to reveal atomic stacking position change in the twin due to the formation of the basal SFs. The results show that, indeed, only those atoms on every other basal plane are displaced by the formation of PSFs, indicating that no global displacement vector can be defined and no dislocation activities are involved in the formation of PSFs. Thus, the proposition of PSF is validated. A special configuration of PSFs was observed, which has limited mobility via coordinated atomic shuffles. A detailed analysis on the structural differences between I_1, I_2 stacking faults and PSFs was provided. The formation mechanism of PSFs can be extended to other HCP metals.

1. Introduction

In crystalline metals, stacking faults (SFs) may form during plastic deformation in which a part of a single crystal is sheared relative to the other part via a partial dislocation. In plastic deformation of face-centered-cubic (FCC) crystal structures, a Shockley partial with a Burgers vector of $\frac{1}{6}\langle 11\bar{2}\rangle$ on the close-packed $\{1\,1\,1\}$ plane is energetically more favorable in terms of energy barrier for slip than a full dislocation with a Burgers vector of $\frac{1}{2}\langle 1\bar{1}0\rangle$ [1–5]. Normally, due to the symmetry of FCC structures, a trailing partial will nucleate and eliminate the SF created by the leading partial. An SF created in this fashion is called I_2 type [6]. The equilibrium width of an I_2 SF, which is the separation between the leading and trailing partial, is inversely proportional to the stacking fault energy (SFE).

SFs can also be created due to generation of excess of vacancies inside a crystal. Irradiation or severe plastic deformation can produce high density vacancies. The vacancies tend to cluster and form vacancy discs on the close-packed planes. Above and below the vacancy discs, the $\{1\,1\,1\}$ planes collapse and form an immobile dislocation loop. Because the displacement vector is perpendicular to the loop plane, this dislocation is immobile. Near the loop plane, large lattice distortion can be observed due to the collapsing. Such loops are usually faulted [7,8] and the corresponding SFs are called I_1 type. The loops are called Frank partials [6].

Configurations of SFs in low symmetry hexagonal close-packed (HCP) crystals are much more complicated. In plastic deformation, formation of SFs on the close-packed basal planes is similar to that in FCC crystals. An I_2 SF is formed on the basal plane and the Burgers vector of a Shockley partial equals $\frac{1}{3}\langle 10\bar{1}0\rangle$. A shear along this direction, which has the lowest energy barrier, gives rise to Shockley partials and the associated basal I_2 SFs. Despite the low SFEs of HCP metals, the equilibrium width of basal SFs is usually on the order a couple of nanometers, thus in conventional transmission electron microscopy

* Corresponding authors.
E-mail address: binl@unr.edu (B. Li).

https://doi.org/10.1016/j.commatsci.2021.110684
Received 3 November 2020; Received in revised form 15 May 2021; Accepted 22 June 2021
Available online 16 July 2021

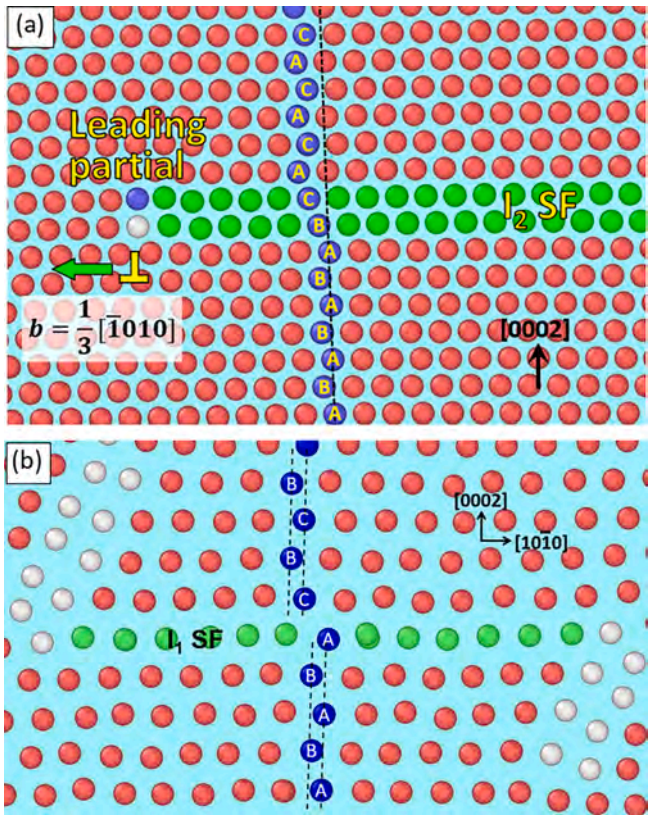

Fig. 1. (a) An I_2 stacking fault (SF) created by a Shockley partial dislocation in Mg. The SF is shown by the two-layer green atoms in common neighbor analysis [9]. Viewing direction $\langle 1\bar{2}10\rangle$. A prismatic plane is pre-selected and colored in blue. After the partial dislocation glides through, all the blue atoms above the slip plane are displaced along the slip direction, in reference to the black dashed line. (b) An I_1 SF created by the collapse of a vacancy disc on the basal plane in Mg (details are provided in Supplemental Material). The SF is shown by the single-layer green atoms. A prismatic plane is pre-selected and colored in blue. After relaxation, the blue atoms above the fault plane are all displaced toward the left, as indicated by the dashed black lines. In both cases, a global displacement vector can be defined. (For interpretation of the references to color in this figure legend, the reader is referred to the web version of this article.)

(TEM) observations, the partial dislocations and the SFs are difficult to resolve.

It is worth noting that for both I_1 and I_2 SFs, a global displacement vector can be defined during the formation of these SFs. To make this point clear and for the convenience of following discussion, we analyze the change in stacking sequence due to the formation of I_1 and I_2 SFs in HCP magnesium (Mg) in atomistic simulations. As shown in Fig. 1a, a leading Shockley partial with a Burgers vector of $\frac{1}{3}\langle 10\bar{1}0\rangle$ is gliding toward left, creating an I_2 SF behind. In common neighbor analysis (CNA) [9], the I_2 SF is displayed as double-layer green atoms. Before the glide of the Shockley partial, atoms on a prismatic plane were pre-selected and colored in blue. Without the I_2 SF, the stacking sequence of these blue atoms is …*ABABAB*…, as shown by the capital letters inside the blue atoms below the SF. However, after the Shockley partial glides through, the stacking sequence changes. Across the I_2 SF, the stacking sequence becomes *ABCA* which is FCC stacking. An important feature in Fig. 1a is that the atoms above the SF plane are *all* displaced by a distance equal to the magnitude of the Burgers vector. This can be seen from the black, dashed line which marks the original position of the prismatic plane and serves as a reference. In Fig. 1b, an I_1 SF was created by collapse of a vacancy disc on the basal plane of Mg (details of the formation process and analysis are provided in Supplemental Material). Similarly, atoms on a prismatic plane were pre-selected and colored in blue. After relaxation, an I_1 SF is formed, as shown by the single-layer green atoms. Across the SF, the stacking sequence is changed from *ABAB* to *ACB* which is also FCC stacking. In Fig. 1b, atomic planes near the I_1 SF are curved due to lattice distortion. Again, it is important to note that the blue atoms above the SF plane are *all* displaced to left by an equal distance. Thus, in these two scenarios, a global displacement vector can always be defined due to the formation of an I_1 or I_2 SF.

SFs on other slip planes such as prismatic planes and pyramidal planes of HCP metals are not well understood despite extensive studies over the past decades. Li and Ma [10] showed that pyramidal slip may preferably occur on $\{10\bar{1}1\}$ planes, creating a wide pyramidal SF. SFs on $\{11\bar{2}2\}$ pyramidal planes as a result of dissociation of a $\frac{1}{3}\langle 11\bar{2}3\rangle$ Burgers vector were proposed and simulated by a number of researchers [11–14], but these SFs have yet been confirmed by experimental observations. Wu and Curtin [14] reported unstable dissociation of pyramidal dislocations onto the basal plane, leading to formation of I_1 basal SFs bounded by two partial dislocations whose Burgers vectors have a component perpendicular to the basal plane. Such a configuration has a very low mobility. Atomic stacking position analysis similar to that in Fig. 1a and b indicates that such SFs are indeed I_1 type.

A special type of basal SFs have been frequently observed in simulations and experiments in deformation of HCP metals, e.g. titanium (Ti), zirconium (Zr), Mg and cobalt (Co) [15–21]. These SFs are formed inside deformation twins, including both $\{10\bar{1}1\}\langle 10\bar{1}2\rangle$ and $\{10\bar{1}2\}\langle 10\bar{1}1\rangle$ twins, but not inside $\{11\bar{2}2\}\langle 11\bar{2}3\rangle$ and $\{11\bar{2}1\}\langle 11\bar{2}6\rangle$ modes. Most of these SFs may cross a whole twin, with both ends connected to the twin boundaries (TBs). As the TBs migrate, the SFs grow wider and wider. The SFs were also observed to terminate at the interior of a twin, with one end attached to a defect inside the twin. Sometimes such a defect presented barely visible diffraction contrast in TEM. These anomalous basal SFs were neither I_1 nor I_2 and were termed "partial stacking faults" (PSF) first by Song and Gray [15] because not all the atoms are displaced by the formation of PSFs. Despite the literature reports, the mechanism for the formation of PSFs remains elusive because it is very difficult to prove that only those atoms on every other basal plane are displaced by the PSFs during deformation.

The purpose of this work is to conduct a detailed analysis on different configurations of PSFs inside $\{10\bar{1}1\}$ and $\{10\bar{1}2\}$ deformation twins in HCP Mg, by using lattice correspondence analysis in atomistic simulations, such that the concept of PSF can be validated. The results provide an unambiguous understanding to the mechanism of PSFs in HCP metals.

2. Simulation method

To simulate $\{10\bar{1}2\}$ TB migration, two single crystals were constructed and bonded together according to $\{10\bar{1}2\}\langle 10\bar{1}1\rangle$ twin orientation relationship, i.e. the misorientation angle equals 86.3°. But, instead of constructing a coherent TB, we constructed a highly incoherent TB such that the initial $\left\{10\bar{1}2\right\}$ TB was parallel to the basal plane of the parent (see atomic plot below). Thus, the TB is close to a B|P interface that has been observed in extensive atomistic simulations and experimental observations [22]. As shown in many TEM observations, $\{10\bar{1}2\}$ TBs can be extremely incoherent [23–28]. The system had a dimension of 50 nm × 27 nm × 25 nm and contained about 950,000 atoms. For simulation of $\{10\bar{1}1\}\langle 10\bar{1}2\rangle$ twinning, no TB was pre-constructed. Instead, a single crystal was constructed and strained in tension along the $\langle 1\bar{1}00\rangle$ direction, i.e. perpendicular to the *c*-axis of the single crystal. The system had a dimension of 30 nm × 20 nm × 15 nm and contained about 300,000 atoms. $\{10\bar{1}1\}\langle 10\bar{1}2\rangle$ twinning was then activated during deformation. During twin nucleation and growth, basal SFs were generated inside the $\{10\bar{1}1\}$ twin.

Embedded Atom Method (EAM) [29,30] type of potential for Mg-Al

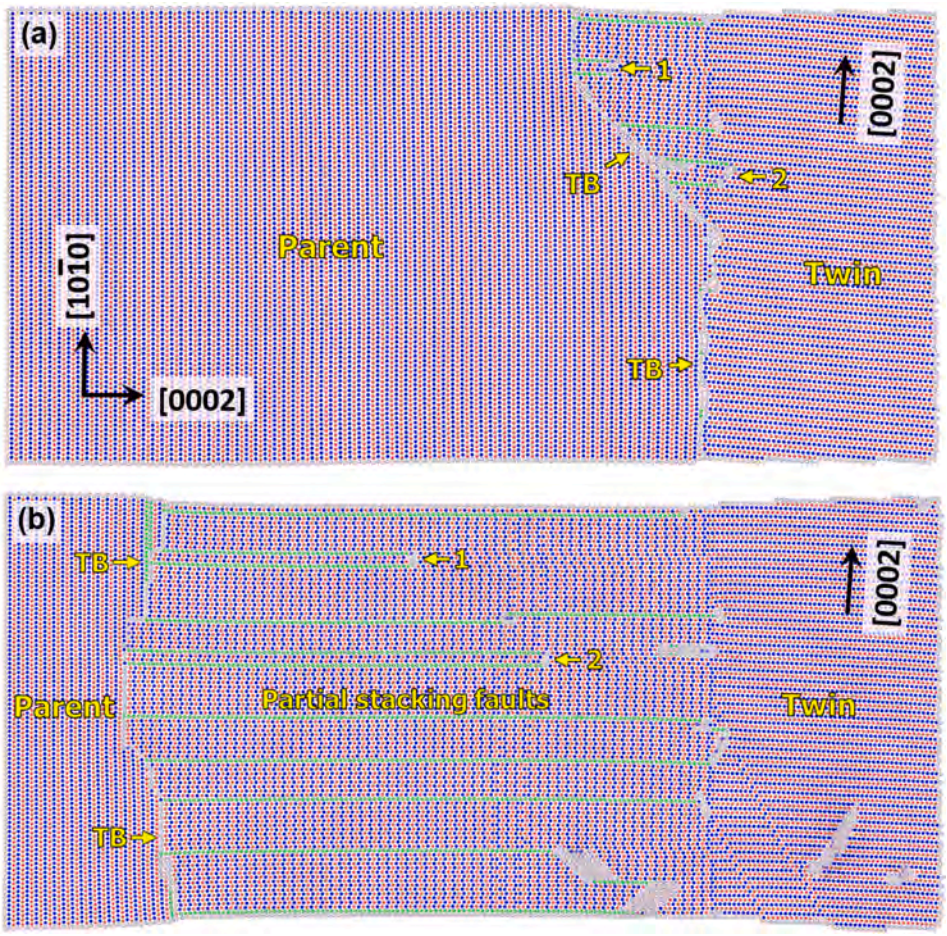

Fig. 2. (a) Basal stacking faults (SFs, colored in green) are being generated as the TB is migrating towards left. One end of the SFs is anchored at the TB and moves along with the TB. Zone axis $\langle 1\bar{2}10\rangle$. The SFs at two locations are marked out to show the motion of the SFs. (b) As the TB is migrating, the right end of the SFs at location 1 slowly moves along. Eventually, the right end of the SFs at location 2 breaks away from the pinning and moves toward left, leading to the decrease in width of the SFs. The SFs at location 1 and 2 appear to be terminating inside the twin. (For interpretation of the references to color in this figure legend, the reader is referred to the web version of this article.)

binary system [31] was used in our simulations. In both simulations, the time step size was 3.5 fs and the system was relaxed for 17.5 ps before the tensile strain was applied. The simulation temperature was maintained at 100 K by applying the Nose-Hoover thermostat [32,33] and the tensile strain rate in the simulations was about 10^8 s^{-1}. No periodic boundary condition was applied. Simulation package XMD for molecular dynamics was used in this work.

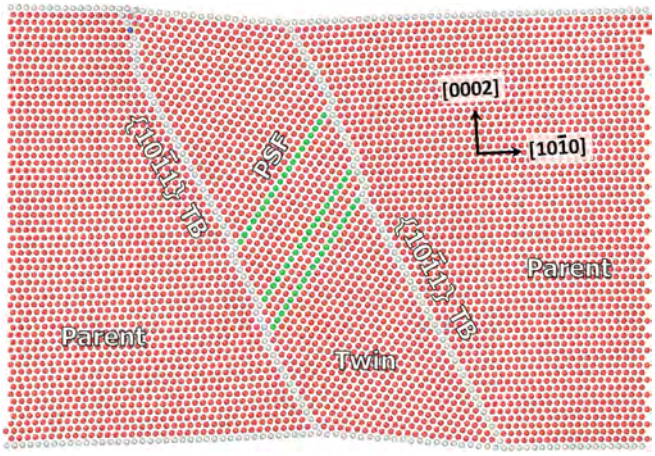

Fig. 3. Basal PSFs (green atoms) are being generated inside a growing $\{10\bar{1}1\}\langle 10\bar{1}\bar{2}\rangle$ twin in atomistic simulations. The SFs cross the whole twin, with both ends anchored at the $\{10\bar{1}1\}$ TBs (gray atoms). The zone axis is along the $[1\bar{2}10]$. As the TBs are migrating, the PSFs grow wider. (For interpretation of the references to color in this figure legend, the reader is referred to the web version of this article.)

Simulations of formation of PSFs inside $\{10\bar{1}2\}$ twins in single crystal Ti and Co during tension along the *c*-axis were also conducted, and the details of simulation method are presented in Supplemental Material.

3. Results

Results from our atomistic simulations of basal SFs inside a $\{10\bar{1}2\}$ twin are shown in Fig. 2. In these plots, the basal planes of the parent and twin are "dyed" alternately in red and blue to represent the basal stacking sequence of HCP structures. This color pattern was retained throughout the simulation. Thus, before and after twinning, how parent planes are transformed to the corresponding planes of the twin can be identified with clarity. Lattice correspondence is a key feature in deformation twinning and solid-state phase transformations [34,35]. As the tensile strain increases, the TB starts migrating toward the parent (Fig. 2a). As the TB migrates, a number of basal SFs (shown as green atoms) on the twin side have been created. In this plot, common neighbor analysis [9] is used to display the atoms of the defects that are not located at the perfect HCP positions (in white). As the TB is migrating, it is composed of coherent segments that are roughly parallel to the $\{10\bar{1}2\}$ plane and incoherent segments that are basal/prismatic type. The right ends of these SFs are attached to the defects that are part of the initial incoherent TB, whereas the left ends are anchored at the migrating TB. As the TB progressively migrates, the basal SFs widen. To compare the positions of the SFs, SFs at two locations 1, 2 are marked out. As the TB migrates, the basal SFs grow wider and wider, as shown in Fig. 2b. As the system is further strained, it can be observed that the right

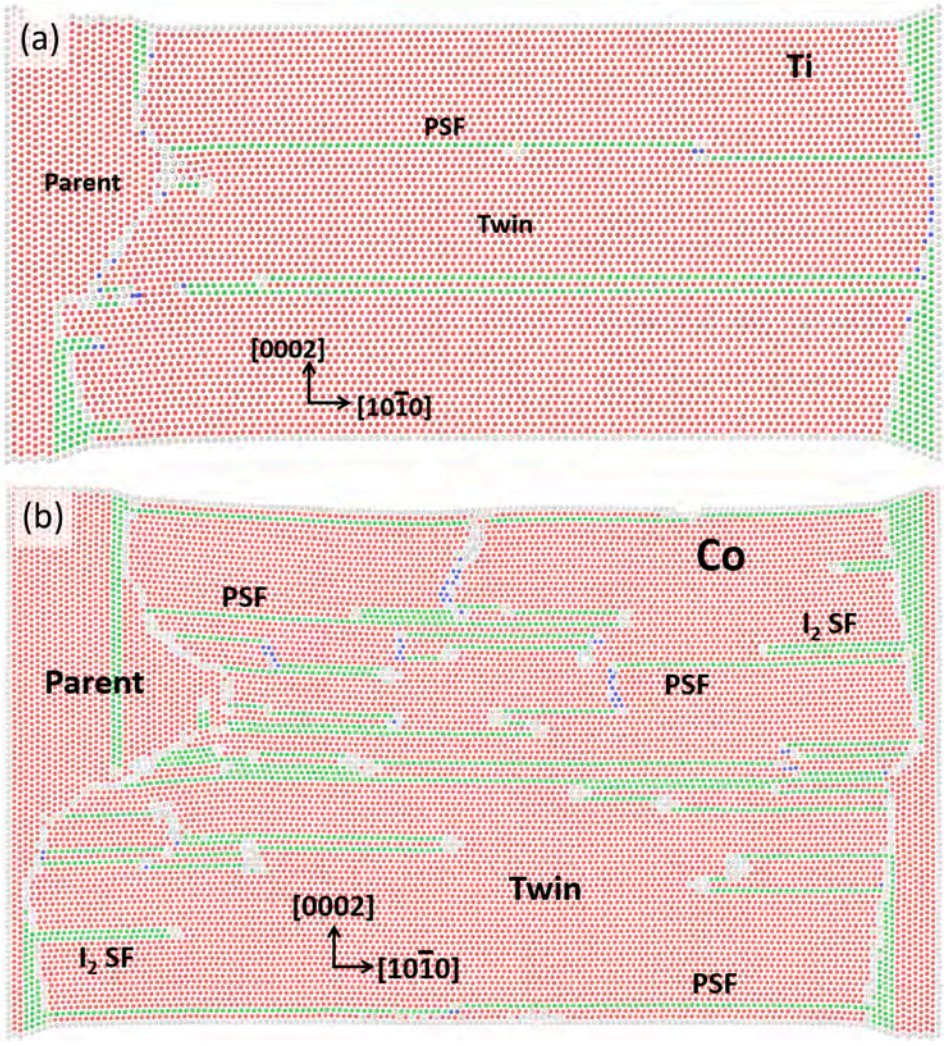

Fig. 4. (a) Wide PSFs are formed inside $\{10\bar{1}2\}$ twin during tension along the *c*-axis of single crystal Ti. (b) Multiple PSFs are formed inside $\{10\bar{1}2\}$ twin during tension along the c-axis of single crystal Co. Multiple I_2 SFs are also formed. Zone axis $\langle 1\bar{2}10\rangle$.

ends of SFs at location 1 are slowly trailing behind the migrating TB (Fig. 2b), indicating that this kind of SF configuration has limited mobility. It is worth noting that the shear factor of these SFs is almost zero, thus the slow motion of the SFs is not related to shear stress. The motion of the right ends partially eliminates the SFs. Meanwhile, more basal SFs are generated along the migrating TB. The right ends of SFs at location 1 almost stop moving. In contrast, the right ends of SFs at location 2 break away from the anchoring defect and move toward the interior of the twin. Eventually, these SFs appear to terminate inside the twin. It can be seen that the SF configuration with limited mobility at location 1 and 2 has a thickness of three layers, i.e. the two SFs (in green) are separated by two layers of basal planes.

The simulation in Fig. 2 was repeated by using the most recent MEAM (Modified Embedded Atom Method [36,37]) potential for Mg developed by Wu and Curtin [14]. This MEAM potential has a better accuracy in terms of stacking fault energy. Similar results were obtained. Thus, irrespective of interatomic potential, wide basal SFs can be formed inside $\{10\bar{1}2\}$ twins.

The migrating $\{10\bar{1}2\}$ TB in Fig. 2 is extremely incoherent in the sense that the TB deviates from the theoretical twinning plane $\left\{10\bar{1}2\right\}$ This is in sharp contrast to the $\left\{10\bar{1}1\right\}$ TB structure as shown in Fig. 3. The TBs (in white) are coherent and perfectly coincide with the $\left\{10\bar{1}1\right\}$ twinning plane. It can be seen that several basal SFs (in green) have formed inside the twin, producing one-layer steps on the TBs (Fig. 3). Both ends of the SFs are attached to the TBs. As the TBs migrates, the twin thickens and the SFs grow wider and wider. It has been shown [17,38] that the growth of $\left\{10\bar{1}1\right\}$ twin is mediated by two-layer or four-layer zonal twinning dislocations. As the partial zonal twinning dislocations glide on the TBs, they pass over and do not react with the one-layer steps. Thus, these one-layer steps on the TBs do not have the characteristics of Shockley partial dislocations. More details on this important feature will be provided below.

Similar results were also obtained in tensile deformation along the *c*-axis of single crystal Ti (Fig. 4a) and Co (Fig. 4b). Wide, one-layer green atoms of basal SFs are formed inside the $\{10\bar{1}2\}$ twins.

4. Analysis and discussion

4.1. Partial displacement in the formation of PSFs

In Fig. 2, wide SFs are generated as a result of TB migration. As shown in Fig. 4, without constructing an initially incoherent TB, if we simply apply a tensile strain along the *c*-axis of a single crystal, $\left\{10\bar{1}2\right\}$ twinning will be activated, and such SFs will also be generated inside the twin (more details are presented in Supplemental Material). In Fig. 3, no

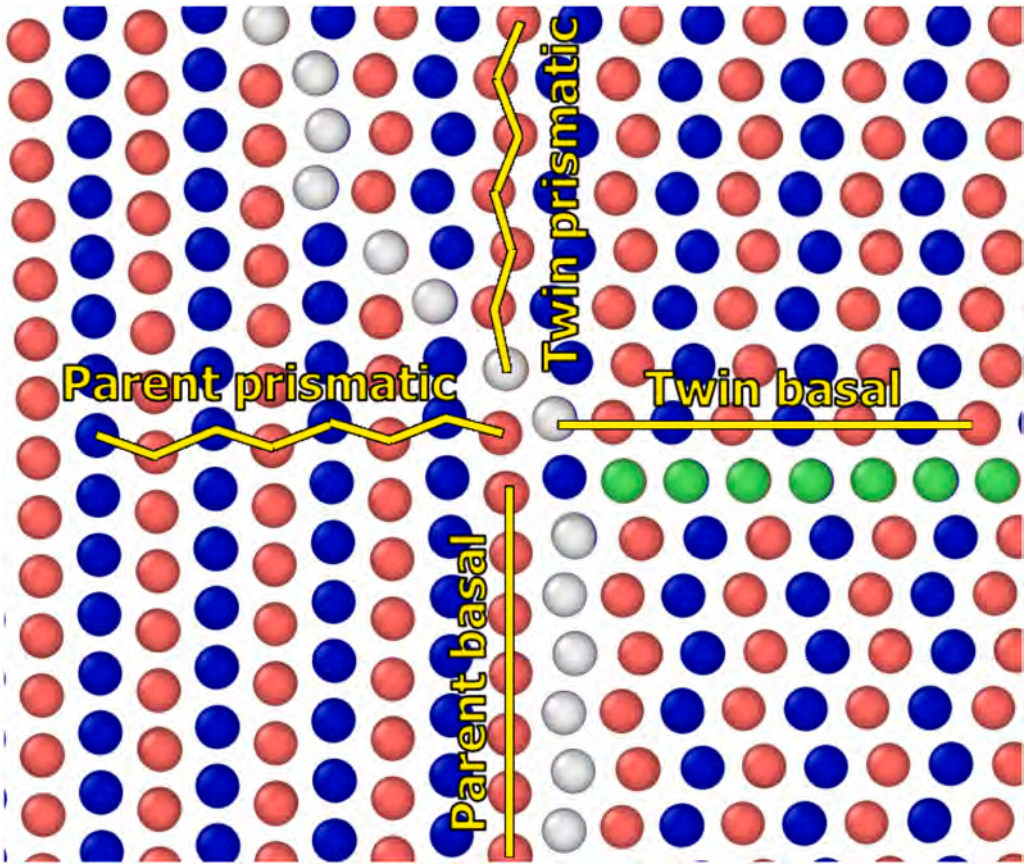

Fig. 5. Lattice correspondence analysis in the simulation of $\{10\bar{1}2\}$ twinning in Mg. It can be seen that the lattice transformation is "parent prismatic to twin basal and parent basal to twin prismatic". The white atoms are TB.

pre-existing TB was constructed, and basal SFs are also generated during $\left\{10\bar{1}1\right\}$ twinning. Thus, the generation of the SFs are only related to the twinning processes themselves.

Wide basal SFs inside $\{10\bar{1}2\}$ twins in Ti and Zr were first reported and systematically studied by Song and Gray [15,39,40]. These anomalous SFs were defined as "partial stacking faults" in the sense that only half of the atoms are displaced by these SFs. Based on their analysis of diffraction contrast, stacking sequence analysis, and the fact that these SFs can be formed over a wide range of experimental conditions irrespective of material, temperature and strain rate, as well as the stacking sequence analysis, Song and Gray concluded that the formation of PSFs was "an integral part of the twinning process in Ti and Zr". Song and Gray also pointed out that the formation of the basal SFs could not be accounted for by twinning dislocation theories. In their experiments, anomalous behavior of $\{10\bar{1}2\}$ twins, such as lack of critical resolved shear stress (CRSS), lack of emissary dislocations and insensitivity to temperature was observed. To interpret the formation of the SFs, they proposed that $\{10\bar{1}2\}$ twinning process was not mediated by a layer-by-layer movement of twinning dislocations, instead, by a "step-wise" or coordinated movement of a large number of atoms between the match planes from the matrix to twin positions. They recognized the significance of atomic shuffling in $\{10\bar{1}2\}$ twinning. In fact, the morphology of the TB in our simulations (Fig. 2) is highly incoherent and changes with simulation time. Such a behavior is a manifestation of the non-dislocation-mediated TB migration for $\{10\bar{1}2\}$ mode. TBs always deviate from the $\{10\bar{1}2\}$ twinning plane and are incoherent, irrespective of the formation of SFs inside the twins [16,23,41]. As a matter of fact, the Song-Gray model is the very first twinning theory that involves no twinning dislocations.

The description of PSFs proposed by Song and Gray [15,39,40], if correct, can be verified in atomistic simulations, which will be presented in the following. Before we discuss the details in our analyses, it is necessary to introduce a crucially important concept in deformation twinning – lattice correspondence which was stated by Christian [42]: "*A deformation which is physically significant implies a one to one correspondence between vectors in the two lattices. Each vector in one lattice may be associated unambiguously with a 'corresponding' vector of the other lattice into which it is converted by the transformation.*" Naturally, this one-to-one correspondence between vectors is applicable to crystallographic planes as well. It follows that an atomic plane of the parent must be transformed to a corresponding plane of the twin. Mathematically, such a lattice transformation can be defined by a second rank tensor, called "lattice correspondence tensor" [42]. For a specific twinning mode, this correspondence tensor C can be inferred by taking into consideration a homogeneous simple shear which can be described by a deformation gradient tensor, and coordinate transformation tensors defined by the parent-twin orientation relationship. In a general form, a vector $\vec{u}$ of the parent is transformed into a corresponding vector $\vec{v}$ of the twin: $\vec{v} = C \cdot \vec{u}$. Based on Christian's description, Niewczas [43] inferred the lattice correspondence tensors for the major twinning modes in HCP metals, and calculated some of the corresponding planes and vectors between parent and twin.

In order to reveal the partial displacements in the formation of the anomalous basal SFs, first we identify the corresponding planes between the parent and the twin in $\{10\bar{1}2\}$ and $\{10\bar{1}1\}$ twinning mode. Because the SFs lie on the basal plane of the twin, the easiest way to examine the displacements of individual atoms caused by the SFs is to track those atoms on a prismatic plane of the twin which is perpendicular to the basal plane. Thus, we select a plane of the parent that has been transformed to the prismatic plane of the twin, track and compare the

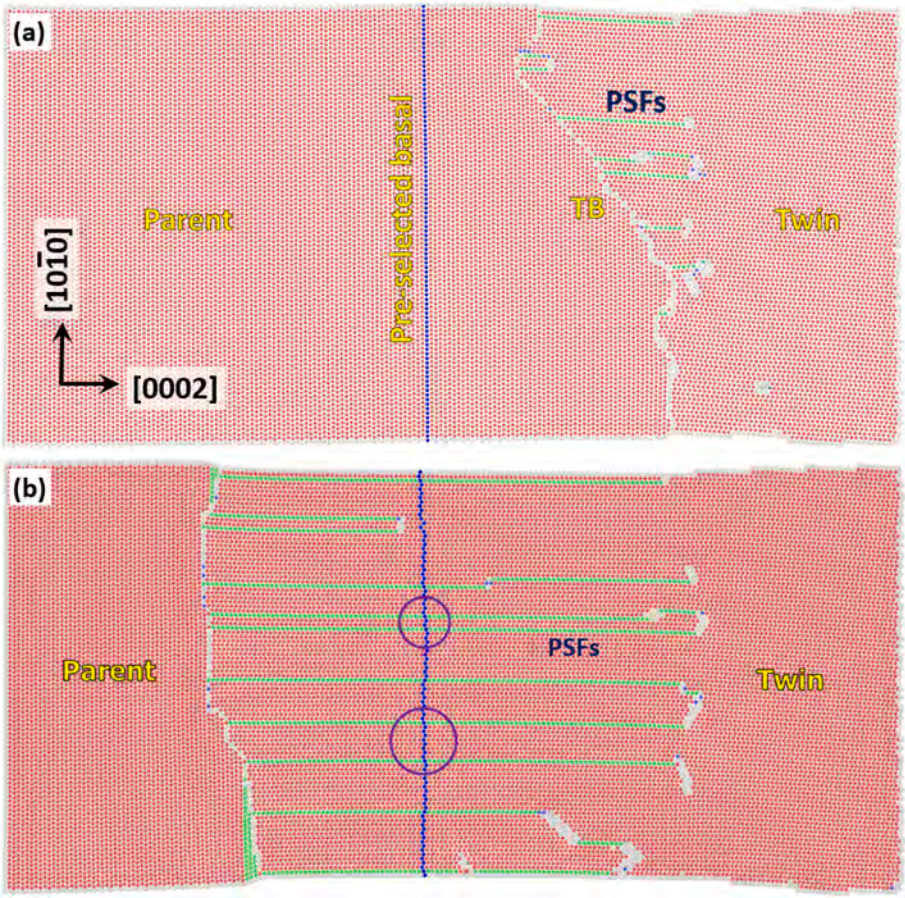

Fig. 6. To reveal the nature of the PSFs, a basal plane of the parent was pre-selected, colored in blue and tracked throughout the simulation. (a) Before the TB traversed through the pre-selected basal. (b) After the TB traversed through, the basal plane was transformed to a prismatic plane of the twin. This lattice correspondence allows analysis of changes in stacking sequence due to the presence of PSFs. Two circled regions are analyzed and shown in Fig. 5. (For interpretation of the references to color in this figure legend, the reader is referred to the web version of this article.)

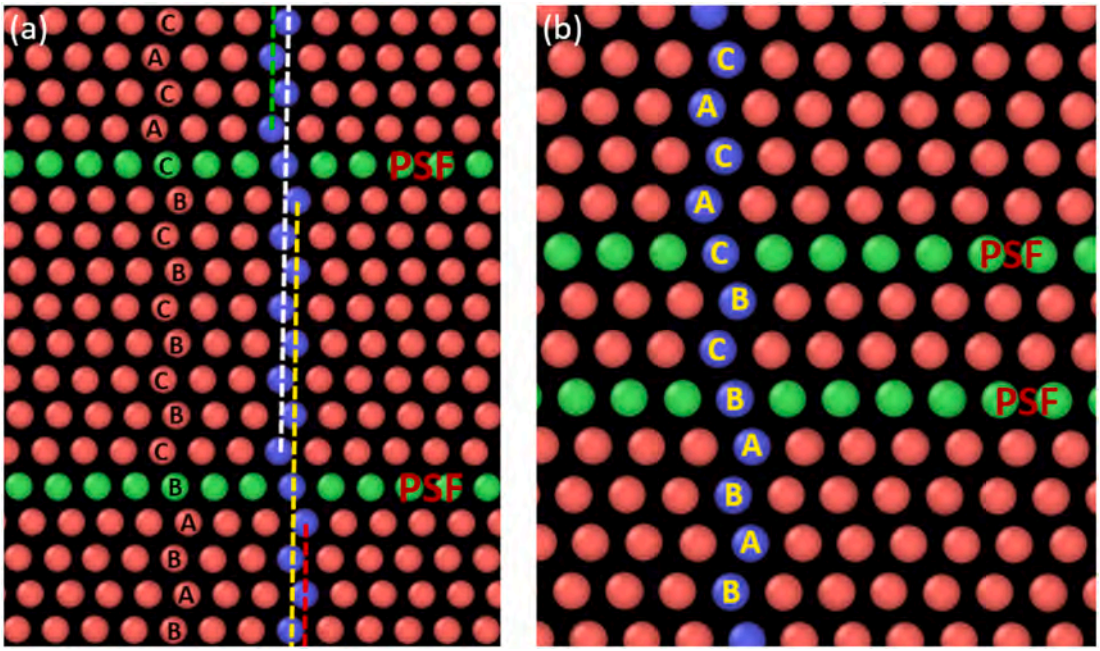

Fig. 7. Close-up views of the circled regions in Fig. 6b. (a) The bottom circle. The blue atoms, which are transformed from a basal plane of the parent and now reside on a prismatic plane of the twin, show that only half of them are displaced due to the presence of the PSFs. Those blue atoms along the yellow and white dashed lines have no relative displacement despite the presence of the PSFs. That is, only every other basal plane are displaced. For instance, to the bottom PSF, the *B* positions remain non-displaced before and after faulting. The capital letters denote the stacking sequence. (b) The top circle. The capital letters indicate partial displacement of the blue atoms: the blue atoms at the *B* positions are not displaced by the bottom PSF. Similarly, the *C* positions are not displaced by the top PSF either. (For interpretation of the references to color in this figure legend, the reader is referred to the web version of this article.)

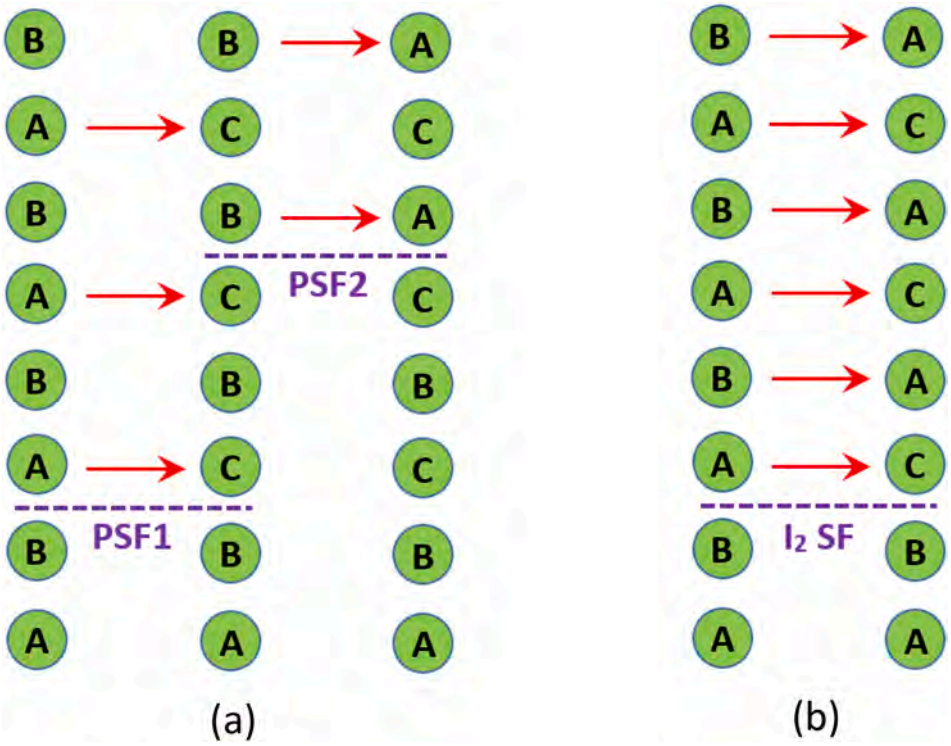

Fig. 8. (a) Schematic of the formation of partially displaced basal PSFs in Figs. 6-7. Only those layers indicated by the red arrows are displaced. (b) In comparison, an I_2 SF is created by a Shockley partial dislocation. Each layer above the SF plane is displaced by a Burgers vector. (For interpretation of the references to color in this figure legend, the reader is referred to the web version of this article.)

structure of the prismatic plane before and after the formation of the SF. According to Niewczas [43], Li and Ma [44], Li and Zhang [24], for $\{10\bar{1}2\}$ mode, a (0002) basal plane of the parent is transformed to a $\{10\bar{1}0\}$ prismatic plane of the twin and a $\{10\bar{1}0\}$ prismatic plane of the parent is transformed to a (0002) basal plane of the twin. This lattice correspondence is clearly shown in Fig. 5 which is a magnified view of the TB in Fig. 2b. Because we assign different colors to the basal planes of the parent, we can easily find out to which planes of the twin these colored basal planes have been transformed during TB migration. It can readily be seen that the lattice correspondence is exactly "parent basal to twin prismatic" and "parent prismatic to twin basal". For $\{10\bar{1}1\}$ mode, a $\{10\bar{1}3\}$ plane of the parent is transformed to a $\{10\bar{1}0\}$ prismatic plane of the twin [43]. Thus, if we track the evolution of a (0002) basal plane of the parent in $\{10\bar{1}2\}$ mode, and a $\{10\bar{1}3\}$ plane of the parent in $\{10\bar{1}1\}$ mode before and after twinning, the nature of the proposed partial displacement can be resolved with clarity.

4.1.1. *PSFs inside* $\{10\bar{1}2\}$ *twins*

Fig. 6 shows how we track a pre-selected (0002) basal plane of the parent which is transformed to a $\{10\bar{1}0\}$ prismatic plane of the twin in the case of Mg. Before twinning, a (0002) basal plane was pre-selected in the middle of the parent crystal before tensile loading. This basal plane, which is an atomically single-layered plane before twinning, was colored in blue and the color of the pre-selected atoms was retained throughout the simulation. After twinning, it can be seen that the originally single-layered plane now becomes a $\{10\bar{1}0\}$ prismatic plane of the twin, which has a double-layered or corrugated structure. The blue prismatic plane intersects with the basal SFs. At the intersections, the stacking sequence of the basal planes changes. Two circled regions are selected for more detailed analysis, as presented below.

The magnified view of the bottom circle in Fig. 6 is shown in Fig. 7a. The two SFs are separated by eight basal planes. The blue atoms are located on a prismatic plane. Indeed, at the intersection between the blue and the red atoms, the stacking sequence is altered by the presence of the basal SFs. An *ABC* stacking and a *BCA* stacking (both are FCC stacking) are present at the two intersections, as shown by the capital letters. An interesting behavior is indicated by the pre-selected blue atoms. Below the bottom SF, a dashed red line and a dashed yellow line are drawn to show that the blue atoms are on the double-layered prismatic plane, and these atoms have a normal stacking sequence of *BABAB* as they should be because this prismatic plane is formed by the pre-selected basal plane of the parent. However, across the bottom SF, although the stacking sequence now becomes *ABC*, the atoms along the yellow dashed line have not changed their positions, i.e. atoms at the *B* positions experience no displacement as opposed to those atoms at the *A* positions, despite the presence of the bottom SF. Between these two basal SFs, the blue atoms are now in *CBCBCBC* stacking, as indicated by the yellow and the white dashed lines which shows the double-layered structure of the prismatic plane. Across the top SF, the stacking sequence changes to *BCA* at the intersection. However, the atoms along the white dashed line have not changed their positions despite the presence of the top SF.

Similar scenario is revealed in Fig. 7b which is a magnified view of the top circled region in Fig. 6b, where the basal SFs have a mobile end with limited mobility. Across the bottom basal SF, the blue atoms at the *B* positions are not displaced by the formation of the SF. Across the top basal SF, the blue atoms at the *C* positions are not displaced by the formation of the top SF.

The detailed analysis in Figs. 6 and 7 clearly indicates that, with the formation of a PSF, only half of the atoms are displaced, and the other half of the atoms are not displaced. This is in stark contrast to I_2 and I_1 SFs (Fig. 1a and b) in which a global displacement vector can always be defined. In both $\{10\bar{1}2\}$ and $\{10\bar{1}1\}$ twinning modes, large atomic shuffles are required and these shuffles play a crucial role in the formation of PSFs. During the formation of PSFs, no global displacement vector can be defined, thus no dislocations can be associated with the formation of these SFs inside $\{10\bar{1}2\}$ and $\{10\bar{1}1\}$ twins.

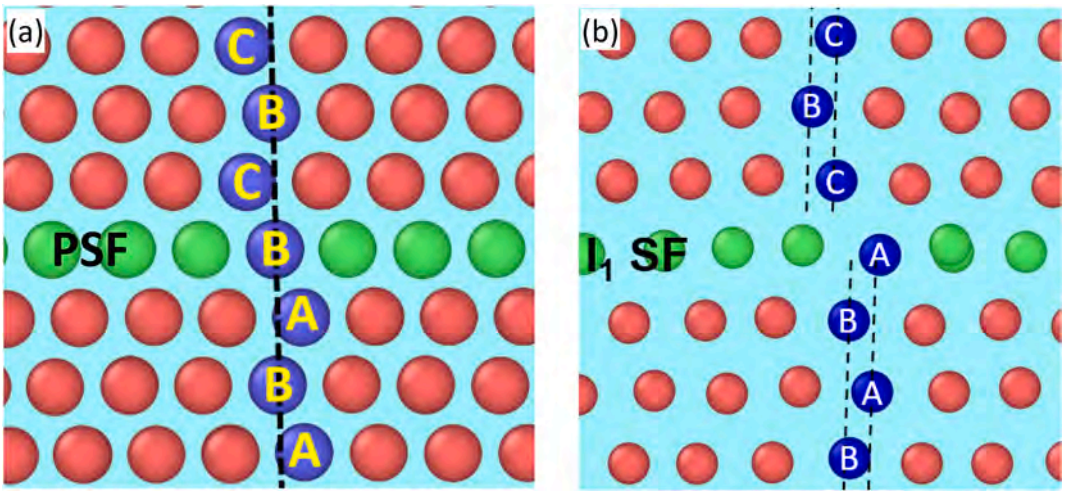

Fig. 9. Comparison between: (a) a PSF and (b) an I_1 SF. Although both SFs are displayed as a single layer of green atoms in common neighbor analysis and their stacking sequence seems the same, for the PSF, atoms at the *B* positions are not displaced by the PSF, i.e. only half of the atoms are displaced, whereas for the I_1 SF, all the atoms above the I_1 SF are displaced. (For interpretation of the references to color in this figure legend, the reader is referred to the web version of this article.)

The difference between the basal SFs with partial displacement and those SFs created by Shockley partial dislocations is further analyzed in Fig. 8. In this analysis we use letter notation to represent stacking sequence. The left column of circles in Fig. 8a represents the normal *ABABABAB* stacking sequence of a perfect HCP lattice. From bottom up, first the *A* layer is displaced to the *C* position, as shown in the middle column in Fig. 8a. This process is accomplished by atomic shuffling and no global displacement is involved. Therefore, the *B* layer remains still and does not move along with the *A* layer. So, only every other basal plane or half of the atoms are displaced due to the formation of the first basal SF (PSF1). A similar scenario takes place at the *B* layer in the middle column of Fig. 8a. The *B* layer is shuffled to the *A* position of the right column of Fig. 8a. In contrast, the *C* layer of the middle column remains still and does not move along with the *B* layer. Thus, a second basal SF (PSF2) is formed.

In contrast, Fig. 8b schematically shows how an I_2 type of basal SF is generated by glide of a Shockley partial dislocation. The left column of circles shows the normal *ABABAB* stacking sequence of perfect HCP lattice. Suppose a Shockley partial is nucleated and glide on the *A* layer (indicated by the first red arrow from the bottom), the partial dislocation displaces the atoms on the *A* layer to the *C* positions. As the partial dislocation glides, each layer above the *A* layer moves along, such that the atoms of the *B* layer are displaced to the *A* positions. Thus, a global displacement vector, which is the Burgers vector of the Shockley partial, can be defined. As a result, an I_2 basal SF is generated. As the leading partial glides, a trailing partial nucleates and eliminates the SF.

For the convenience of comparison, magnified views of the local structure across a PSF and an I_1 SF are displayed side by side in Fig. 9. For both PSF and I_1 SF, they all are displayed as a single layer of green atoms in the common neighbor analysis. Above and below both SFs, the stacking sequence seems the same. However, For the PSF (Fig. 8a), across the PSF, those atoms at the B positions are not displaced by the formation of the PSF. They remain on the same column, as indicated by the vertical dashed black line. Only those atoms at the C positions are displaced to the left. In contrast, for the I_1 SF (Fig. 9b), those atoms above the SF are *all* displaced to left, as indicated by the double black, dashed lines. Thus, similar to an I_2 SF (Fig. 1a), a global displacement vector can be defined as well for an I_1 SF.

The equilibrium width of an I_2 SF is a result of the balance between the repulsive force of the leading and trailing partial (mechanical energy) and the SF energy (chemical energy). The equilibrium width of an I_2 SF is on the order of $1 \sim 3$ nm in pure Mg and slightly varies with the dislocation characteristics in terms of edge or screw or mixed [45–47].

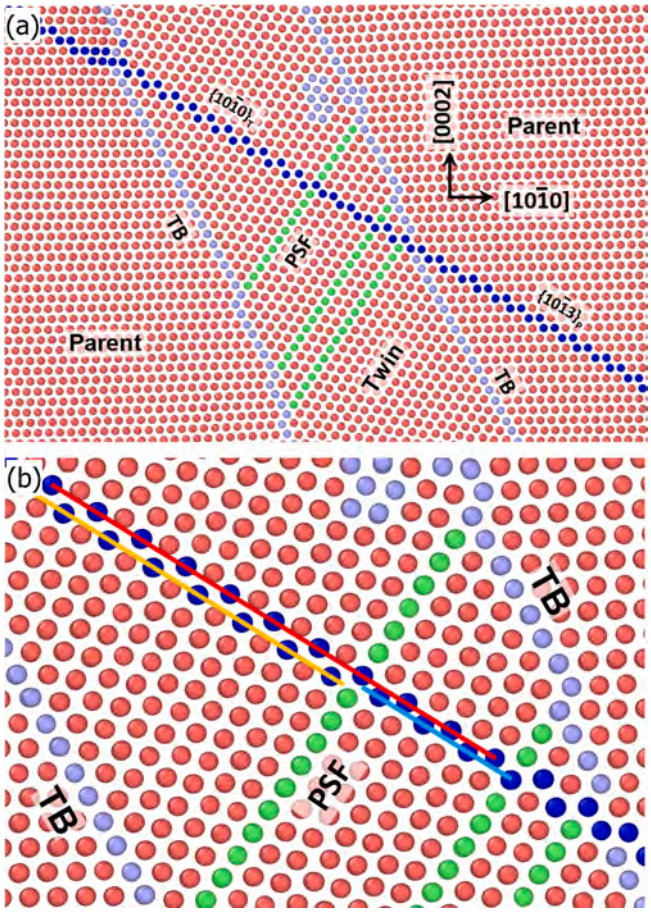

Fig. 10. (a) Basal PSFs (in green) are also observed in atomistic simulations of $\{10\bar{1}1\}\langle 10\bar{1}2\rangle$ twinning. To reveal the partial displacement, atoms of a parent $\{10\bar{1}3\}_P$ plane (in blue) were pre-selected before twinning. After twinning, the $\{10\bar{1}3\}_P$ plane was transformed to the $\{10\bar{1}0\}_T$ plane of the twin. (b) A magnified view of the basal PSFs and the blue atoms on the $\{10\bar{1}0\}_T$ plane in (a). It is clear that the blue atoms on the red line are not displaced by the presence of the PSF. Only those blue atoms on the blue line are displaced and now on the yellow line. (For interpretation of the references to color in this figure legend, the reader is referred to the web version of this article.)

In contrast, PSFs are non-equilibrium defects that involve no partial dislocations, and their widths can be three to four orders of magnitude wider than that of I_2 SFs. It is not unusual that a $\{10\bar{1}2\}$ twin can consume a whole grain, thus, PSFs can run through a whole grain when it is totally twinned. As for I_1 SFs, their widths are dependent upon vacancy density and temperature, and these SFs are typically associated with lattice distortion near the fault plane.

4.1.2. *PSFs inside* $\{10\bar{1}1\}$ *twins*

Next, we analyze the nature of partial displacement of the basal SFs inside the $\{10\bar{1}1\}$ twin and the analysis is presented in Fig. 10a. First, we pre-selected a $\{10\bar{1}3\}$ plane of the parent and colored the atoms on this plane in blue. According to [38,43], this $\{10\bar{1}3\}$ plane of the parent is transformed to the $\{10\bar{1}0\}$ prismatic plane of the twin. The position of the $\{10\bar{1}3\}$ plane of the parent is carefully pre-selected such that after twinning, the corresponding $\{10\bar{1}0\}$ prismatic plane of the twin intersects the basal SFs. This lattice transformation can be seen from the blue atoms inside the twin. Indeed, after twinning, across the TB, the blue $\{10\bar{1}3\}$ plane of the parent has transformed to a $\{10\bar{1}0\}$ prismatic plane of the twin.

To show the partial displacement caused by the PSFs, we magnify the region where the blue atoms intersect the SFs, as shown in Fig. 10b. Three lines in red, blue and yellow are drawn to denote the positions of the blue atoms on both sides of the SFs. The red and the blue lines indicate the double-layered structure of the prismatic plane of the twin. It can be seen that the blue atoms along the red line experience no position change with the presence of the basal SF. That is, on both sides of the SF, the stacking positions of the blue atoms remain the unchanged. In contrast, those blue atoms along the blue line have changed their positions across the SF, and they are now residing along the yellow line which is a neighboring prismatic plane of the one denoted by the red line. Recently, Zhou and Sui [48] studied high density SFs inside $\{10\bar{1}1\}$ twins in deformed Mg alloys, using Cs-corrected TEM. Their HRTEM images clearly show that the stacking sequence of the SFs is indeed characteristic of PSFs.

With clarity, our analysis (Figs. 6–10) indicates that the anomalous basal SFs that are formed inside $\{10\bar{1}2\}$ and $\{10\bar{1}1\}$ twins in HCP metals are not generated by activities of partial dislocations because only half of the atoms or atoms on every other basal plane are displaced by the SFs. This is consistent with the description of Song and Gray [15,39,40]. Thus, the concept of "partial stacking faults" is validated. As shown by Zhang et al. [16] and Sun et al. [17], the formation of these SFs are closely related to large atomic shuffles that are involved in TB migration in these two twinning modes.

It is well known that, large shuffles are indispensable in $\{10\bar{1}2\}$ and $\{10\bar{1}1\}$ twinning modes in HCP metals because a homogeneous simple shear is unable to carry all the parent atoms to the twin positions [42]. The necessity of large shuffles can easily be seen in Fig. 5. For $\{10\bar{1}2\}$ mode, a basal plane of the parent must be transformed to a prismatic plane of the twin, and vice versa. This lattice transformation has been revealed in almost all atomistic simulations in the published works, despite the claimed twinning dislocation, disconnection and disclination at TBs [22,49,50]. However, atomically, a basal plane has a single-layered structure whereas a prismatic plane has a double-layered structure. Thus, atomic shuffles must be involved in such a transformation between the two corresponding planes. The largest shuffle is about four times the magnitude of the theoretical Burgers vector of the elementary twinning dislocation [51–53]. As shown by Li and Zhang [52], the $\{10\bar{1}2\}$ twinning plane cannot remain invariant during lattice transformation, thus the magnitude of twinning shear should be zero. This is the very reason that accounts for incoherent TB migration mediated purely by atomic shuffling [54]. Atoms may shuffle and land on faulted positions, resulting in formation of anomalous basal SFs, but only every other basal plane is displaced by such SFs. For $\{10\bar{1}1\}$ mode,

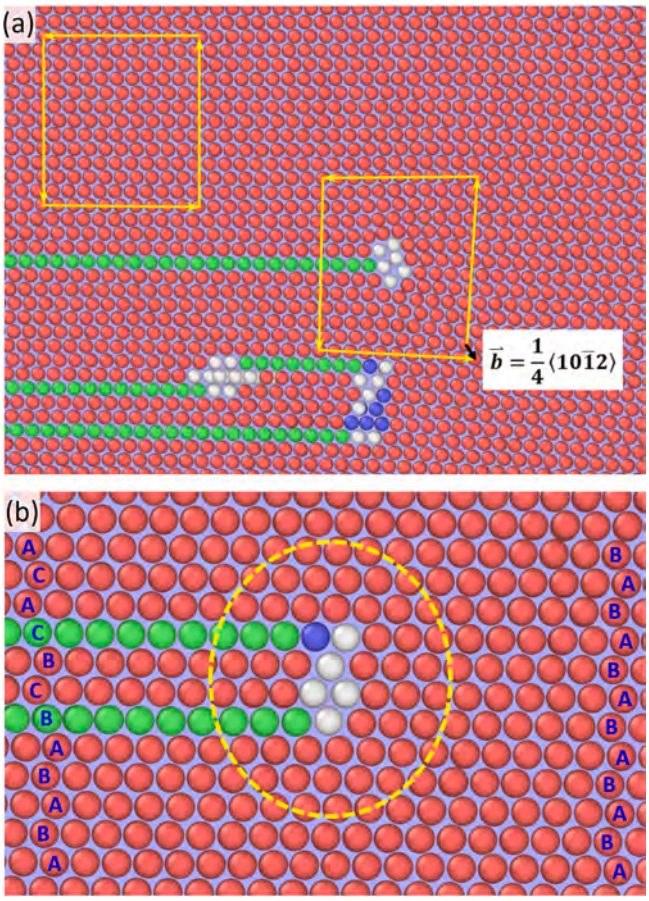

Fig. 11. (a) Burgers vector analysis for location 2 in Fig. 2, where the PSF is pinned at the right end and only the left end is moving with the TB. The Burgers vector (indicated by the black arrow) equals $\frac{1}{4}\langle 10\bar{1}2\rangle$, which has a $\langle c\rangle$ component. In this case, the PSF is firmly pinned by the defect at the right end. (b) A close-up of the PSFs at location 1 with a mobile right end that terminates inside the twin. The two PSFs are connected by the blue and the gray atoms (the circled region). In this configuration, the lattice distortion in the circled region is minimal. (For interpretation of the references to color in this figure legend, the reader is referred to the web version of this article.)

the twinning mechanism is different in the sense that a homogeneous simple shear does occur on the $\{10\bar{1}1\}$ twinning plane, and zonal twinning dislocations are involved in TB migration [38]. As shown in Fig. 10a, a $\{10\bar{1}3\}$ plane of the parent is transformed to a $\{10\bar{1}0\}$ plane of the twin. Also, a (0002) basal plane of the parent is transformed to a $\{10\bar{1}\bar{1}\}$ plane of the twin [17,38]. During these transformations, shuffles as large as $\frac{1}{2}a_0$ (a_0 is the lattice parameter. For Mg, a_0 equals 0.321 nm) must be involved, with a magnitude of about five times the Burgers vector of the elementary twinning dislocation. The direction of these extraordinarily large shuffles is nearly perpendicular to the direction of twinning shear. Despite the glide of zonal twinning dislocations on the coherent TBs, when atoms shuffle and land on faulted positions, PSFs are produced.

4.2. *PSF configuration with a mobile end*

Our atomistic simulations indicate that there are two types of basal SFs inside $\{10\bar{1}2\}$ and $\{10\bar{1}1\}$ twins of HCP metals. One type is the majority of the SFs that may cross the whole twin lamella, with both ends anchored at the migrating twin boundaries. The other type is those that may terminate in the interior of the twin lamella, but the end inside the twin must be attached to a defect (Fig. 11). Our atomistic simulations

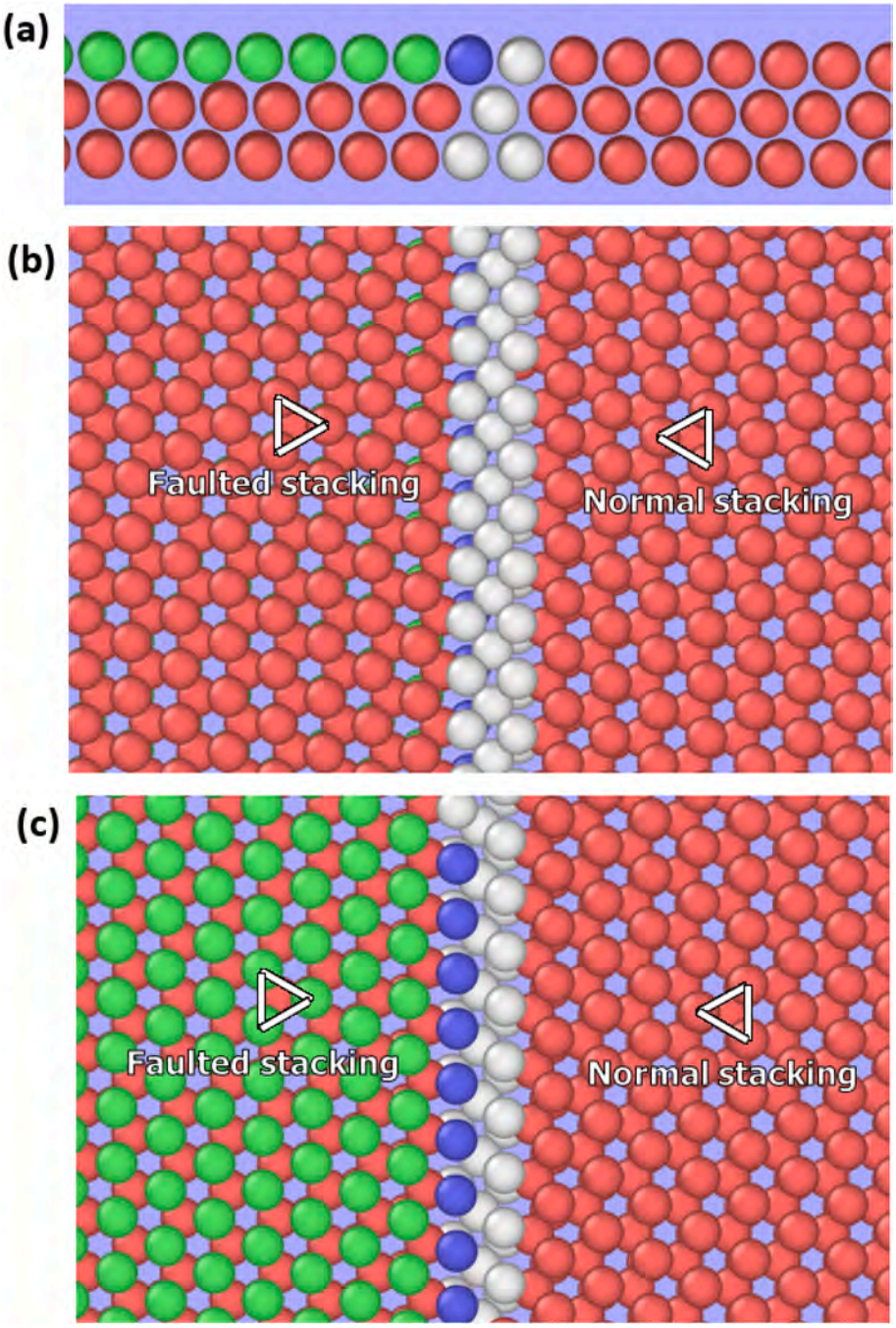

Fig. 12. (a) Three atomic layers are shown in a close-up of the right end of the PSFs in Fig. 11. The gray and blue atoms separate these atomic planes into two regions that have different stacking sequence. (b) Bottom view of (a). The difference in the stacking sequence on both sides is obvious. The gray atoms have a different structure than normal HCP. (c) Top view of (a). The top layer, which contains the green and the red atoms, as well as the blue and gray atoms that separate the green and the red atoms, has a nearly normal hexagonal structure across the entire layer, except for minor distortions in the central area that separates the green and the red atoms. (For interpretation of the references to color in this figure legend, the reader is referred to the web version of this article.)

also show that a special configuration of the basal SFs has limited mobility at one end (location 1 and 2 in Fig. 2). Fig. 11a shows the magnified view near location 2 in Fig. 2a. The yellow circuits indicate that the Burgers vector of the dislocation (represented by the gray atoms) equals $\frac{1}{4}\langle 10\bar{1}2\rangle$. The defect configuration at location 2 is more complex because it involves more than two basal planes. Such a configuration has a strong pinning effect on the PSFs.

As shown in Fig. 2b, the basal SFs with one end that has limited mobility always contain three basal planes. In the following we closely examine the structure of such an SF configuration. Fig. 11b shows a close-up of the SFs at location 1 in Fig. 2a. The right ends of the PSFs are connected by the white and blue atoms which have neither HCP nor FCC structure. It can be seen that the presence of the three-layer faulted region produces minimal lattice distortion inside the yellow circle. To the right of the circle, the normal *ABABAB* stacking sequence of the twin is marked out by the capital letters. To the left of the circle, the stacking sequence has changed due to the presence of the PSFs. At both PSFs, the HCP stacking has changed to FCC stacking. Above the top PSF, the stacking sequence has changed to *CACACA*, as compared to the *ABABAB* normal stacking. Structurally, these two stacking sequences are equivalent. Hence, the bottom PSF changes the stacking sequence, but the top PSF restores the sequence to the normal stacking, despite the change in notation. At the bottom PSF, the stacking sequence changes from *ABABABA* to *ABABABC*. Thus, as shown by the capital letters, the *B* layers actually do not change their positions with the presence of the bottom SF. Similarly, the *C* layers do not change their positions with the presence of the top SF. This is an important characteristic of the PSFs inside $\left\{10\bar{1}2\right\}$ and $\{10\bar{1}1\}$ twins of HCP metals.

Like dislocations which cannot terminate inside a perfect crystal and

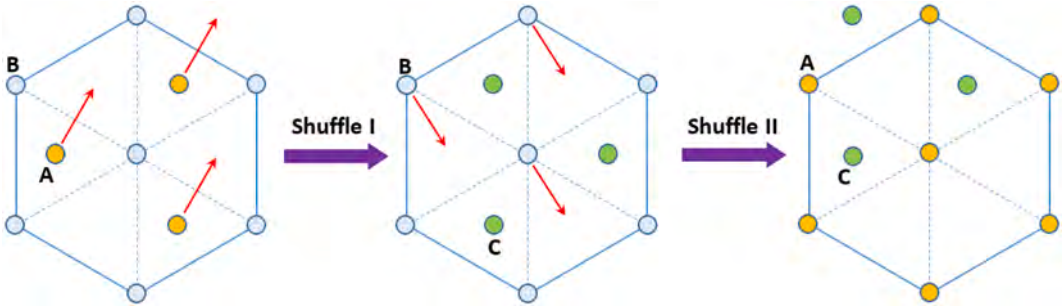

Fig. 13. Illustration of change in stacking sequence due to shuffles that only displace every other basal plane. Shuffle I changes …*BABA*… stacking to …*BCBC*… stacking. The A positions shuffle to the C positions but the B positions stay unchanged. Shuffle II changes …*BCBC*… stacking to …*ACAC*… stacking which is structurally identical to …*BABA*… stacking. The B positions shuffle to the A positions but the C positions stay unchanged. Thus, two serial shuffling processes recover the stacking sequence, despite the notation change.

can only terminate at grain boundaries, surfaces, interfaces or other crystalline defects or form dislocation loops, the PSFs in the interior of a twin must terminate at a certain defect as well. Thus, there must be a boundary that separates the normal stacking region from the faulted region, and the boundary is the white and blue atoms in Fig. 11. To examine this structure, we select three layers of the basal planes near the circled region, i.e. the top green layer and the two red layers below it. A magnified view of these basal planes is shown in Fig. 12a. The bottom view and the top view of the layers are shown in Fig. 12b and c, separately. In the bottom view (Fig. 12b), two triangles are drawn to denote the characteristic stacking in the normal and the faulted region. Between the two regions are the white atoms with a disordered structure that differs from HCP structure, indicative of relatively large lattice distortion. Close examination reveals that the red atoms in the faulted region are shifted downward with respect to the normal stacking region. In the top view (Fig. 12c), the difference in the stacking sequence of the normal and the faulted regions remains the same, but the lattice distortion around the blue atoms is not as significant as the gray atoms in Fig. 12b.

The above analysis can be schematically described in Fig. 13 which shows the change in stacking sequence caused purely by atomic shuffling. As demonstrated above, the PSFs inside $\left\{10\bar{1}2\right\}$ and $\{10\bar{1}1\}$ twins are not produced by glide of Shockley partial dislocations, instead, they are produced by atoms that shuffle to the faulted positions during TB migration. First, the *A* layer shuffles to the position of the *C* layer, as indicated by the red arrows. However, the *B* layer does not move along and stays still. This process is denoted as Shuffle I in Fig. 13 and creates the bottom PSF in Fig. 11b. The stacking sequence changes from …*BABA*… to …*BCBC*…. Second, the *B* layer shuffles to the position of the *A* layer, whereas the *C* layer does not move along. This process is denoted as Shuffle II and creates the top SF in Fig. 10. The stacking sequence changes from …*BCBC*… to *ACAC*…. The final structure after Shuffle II is identical to the normal stacking despite the change in notation.

The white atoms (Fig. 11b) that separate the faulted stacking region from the normal stacking region can only move in a coordinated fashion to eliminate the basal SFs. Thus, their movement is accomplished by local shuffling rather than by a global displacement, and are rather sluggish. The tensile stress is nearly parallel to the PSFs, thus, the shear factor of the PSFs is close to zero. In normal dislocation glide, a critical shear stress is required to overcome the frictional barrier. Hence, the driving force for the limited mobility is the reduction of energy produced by the PSFs, rather than shear stress. I_1 SFs cannot move this way. Additionally, the overall lattice distortion around the white and the blue atoms is insignificant. Thus, in TEM analysis, as shown by Song and Gray [15], the defect associated with the SFs can almost be invisible. Song and Gray [15] also suggested that the SFs may only move by diffusion. From Fig. 11, the coordinated movement of the white atoms differs from diffusion which has to involve vacancies. It can be obviously seen from our simulations that the motion of the SFs involves no vacancies. Actually, the coordinated motion is very similar to detwinning in Al which has a very high SFE (~120 mJ/m^2) [55]. Because of the high SFE, when the external load is removed, nano-twins in pure Al will shrink and eventually disappear. The detwinning process is accomplished by simultaneous movement of atoms on the two neighboring {1 1 1} planes inside a nano-twin. Such a movement is able to reverse the faulted stacking of three consecutive {1 1 1} planes of the twin back to the normal stacking without involving large, local elastic strains.

5. Conclusions

In this work, we present atomistic simulations and analyze in great detail the configurations of wide basal SFs inside $\{10\bar{1}2\}$ and $\{10\bar{1}1\}$ twinning modes in HCP Mg, Ti and Co. The following conclusions can be reached:

(1) Lattice correspondence analysis for $\{10\bar{1}2\}$ and $\{10\bar{1}1\}$ twinning modes unambiguously reveals that, only half of the atoms, or atoms on every other basal plane are displaced when the PSFs are formed. This is consistent with the descriptions by Song and Gray [15] in which the anomalous basal SFs were first defined as "partial stacking faults".
(2) Our results further demonstrate that the formation of PSFs inside $\{10\bar{1}2\}$ and $\{10\bar{1}1\}$ twins is a result of large atomic shuffles that are inevitably involved in these two twinning modes, and has nothing to do with the activities of partial dislocations. The difference between I_1, I_2 and PSF are clarified on the atomic scale. For I_1 and I_2 SFs, a global displacement vector can be defined, whereas for PSFs, no global displacement vector can be defined.
(3) The PSFs can terminate in the interior of the twins with one end attached to a lattice defect. When the SFs form a special configuration, i.e. two PSFs are separated by three basal planes, the two PSFs can be connected by a joint end which has limited mobility. The joint end can move in a sluggish fashion such that the width of the PSFs and the excess energy produced by the PSFs are reduced. Such a motion is achieved by coordinated atomic shuffles and no glide of partial dislocations is involved.

Declaration of Competing Interest

The authors declare that they have no known competing financial interests or personal relationships that could have appeared to influence the work reported in this paper.

Acknowledgements

B. Li is grateful for the support from U.S. National Science Foundation (CMMI-1635088, CMMI-2016263, and CMMI-2032483). X.Y. Zhang acknowledges the support from the National Natural Science

Foundation of China (Grant No. 51271208, 51671040, 50890170 and 51421001) and the Basic Research of China (No. 2010CB631004). Q. Sun thanks supports from National Natural Science Foundation of China (No. 51801165) and Sichuan Science and Technology Program (No. 2020YFH0088). Part of this work used the Extreme Science and Engineering Discovery Environment (XSEDE) [56], which is supported by National Science Foundation grant number ACI-1548562, on Bridges Pylon at Pittsburgh Supercomputing Center through TG-MAT200001.

Appendix A. Supplementary data

Supplementary data to this article can be found online at https://doi.org/10.1016/j.commatsci.2021.110684.

References

[1] V. Vítek, Intrinsic stacking faults in body-centred cubic crystals, Philos. Mag. 18 (1968) 773–786, https://doi.org/10.1080/14786436808227500.
[2] E.B. Tadmor, N. Bernstein, A first-principles measure for the twinnability of FCC metals, J. Mech. Phys. Solids. 52 (2004) 2507–2519, https://doi.org/10.1016/j.jmps.2004.05.002.
[3] S. Kibey, J.B. Liu, D.D. Johnson, H. Sehitoglu, Predicting twinning stress in fcc metals: linking twin-energy pathways to twin nucleation, Acta Mater. 55 (2007) 6843–6851, https://doi.org/10.1016/j.actamat.2007.08.042.
[4] B. Li, B.Y. Cao, K.T. Ramesh, E. Ma, A nucleation mechanism of deformation twins in pure aluminum, Acta Mater. 57 (2009) 4500–4507, https://doi.org/10.1016/j.actamat.2009.06.014.
[5] D. Rodney, L. Ventelon, E. Clouet, L. Pizzagalli, F. Willaime, Ab initio modeling of dislocation core properties in metals and semiconductors, Acta Mater. 124 (2017) 633–659, https://doi.org/10.1016/j.actamat.2016.09.049.
[6] J.P. Hirth, J. Lothe, Theory of Dislocations, second ed., Krieger Publishing Company, 1983.
[7] S.J. Zinkle, L.E. Seitzman, W.G. Wolfer, I. Energy calculations for pure metals, Philos. Mag. A. 55 (1987) 111–125, https://doi.org/10.1080/01418618708209803.
[8] X.L. Wu, B. Li, E. Ma, Vacancy clusters in ultrafine grained Al by severe plastic deformation, Appl. Phys. Lett. 91 (2007), 141908, https://doi.org/10.1063/1.2794416.
[9] A. Stukowski, Visualization and analysis of atomistic simulation data with OVITO–the Open Visualization Tool, Model. Simul. Mater. Sci. Eng. 18 (2010), 015012, https://doi.org/10.1088/0965-0393/18/1/015012.
[10] B. Li, E. Ma, Pyramidal slip in magnesium: dislocations and stacking fault on the 10–11 plane, Philos. Mag. 89 (2009) 1223–1235, https://doi.org/10.1080/14786430902936707.
[11] Y. Minonishi, S. Ishioka, M. Koiwa, S. Morozumi, Motion of a 1/3⟨1123⟩ screw dislocation in a model h.c.p. lattice, Philos. Mag. A. 46 (1982) 761–770, https://doi.org/10.1080/01418618208236929.
[12] M.H. Liang, D.J. Bacon, Computer simulation of dislocation cores in h.c.p. metals II. Core structure in unstressed crystals, Philos. Mag. A. 53 (1986) 181–204, https://doi.org/10.1080/01418618608242820.
[13] J.R. Morris, J. Scharff, K.M. Ho, D.E. Turner, Y.Y. Ye, M.H. Yoo, Prediction of a 1122 hcp stacking fault using a modified generalized stacking-fault calculation, Philos. Mag. A. 76 (1997) 1065–1077, https://doi.org/10.1080/01418619708200015.
[14] Z. Wu, W.A. Curtin, The origins of high hardening and low ductility in magnesium, Nature 526 (2015) 62–67, https://doi.org/10.1038/nature15364.
[15] S.G. Song, G.T. Gray, Transmission electron microscopy examination and analysis of an anomalous stacking fault in h.c.p. metals, Philos. Mag. A. 71 (1995) 263–274, https://doi.org/10.1080/01418619508244355.
[16] X. Zhang, B. Li, Q. Liu, Non-equilibrium basal stacking faults in hexagonal close-packed metals, Acta Mater. 90 (2015) 140–150.
[17] Q. Sun, Q. Zhang, B. Li, X. Zhang, L. Tan, Q. Liu, Non-dislocation-mediated basal stacking faults inside {10-11}<10-1-2> twins, Scr. Mater. 141 (2017) 85–88, https://doi.org/10.1016/j.scriptamat.2017.07.036.
[18] Y. Tang, J.A. El-Awady, Formation and slip of pyramidal dislocations in hexagonal close-packed magnesium single crystals, Acta Mater. 71 (2014) 319–332, https://doi.org/10.1016/j.actamat.2014.03.022.
[19] H. Fan, J.A. El-Awady, Towards resolving the anonymity of pyramidal slip in magnesium, Mater. Sci. Eng. A. 644 (2015) 318–324, https://doi.org/10.1016/j.msea.2015.07.080.
[20] A. Ostapovets, A. Serra, Slip dislocation and twin nucleation mechanisms in hcp metals, J. Mater. Sci. 52 (2017) 533–540, https://doi.org/10.1007/s10853-016-0351-4.
[21] H. Pan, Q. Huang, G. Qin, H. Fu, M. Xu, Y. Ren, J. She, B. Song, B. Li, Activations of stacking faults in the calcium-containing magnesium alloys under compression, J. Alloys Compd. 692 (2017) 898–902, https://doi.org/10.1016/j.jallcom.2016.09.128.
[22] J.P. Hirth, J. Wang, C.N. Tomé, Disconnections and other defects associated with twin interfaces, Prog. Mater. Sci. 83 (2016) 417–471, https://doi.org/10.1016/j.pmatsci.2016.07.003.
[23] X.Y. Zhang, B. Li, X.L. Wu, Y.T. Zhu, Q. Ma, Q. Liu, P.T. Wang, M.F. Horstemeyer, Twin boundaries showing very large deviations from the twinning plane, Scr. Mater. 67 (2012) 862–865, https://doi.org/10.1016/j.scriptamat.2012.08.012.
[24] B. Li, X.Y. Zhang, Twinning with zero twinning shear, Scr. Mater. 125 (2016) 73–79, https://doi.org/10.1016/j.scriptamat.2016.07.004.
[25] P.G. Partridge, E. Roberts, The formation and behaviour of incoherent twin boundaries in hexagonal metals, Acta Metall. 12 (1964) 1205–1210, https://doi.org/10.1016/0001-6160(64)90103-8.
[26] M.A. Gharghouri, G.C. Weatherly, J.D. Embury, The interaction of twins and precipitates in a Mg-7.7 at.% Al alloy, Philos. Mag. A. 78 (1998) 1137–1149, https://doi.org/10.1080/01418619808239980.
[27] X.Y. Zhang, B. Li, J. Tu, Q. Sun, Q. Liu, Non-classical twinning behavior in dynamically deformed cobalt, Mater. Res. Lett. 3 (2015) 142–148, https://doi.org/10.1080/21663831.2015.1034297.
[28] X.Y. Zhang, B. Li, Q. Sun, On the 10–12 "twinning shear" measured from line deflection, Scr. Mater. 159 (2019) 133–136, https://doi.org/10.1016/j.scriptamat.2018.09.027.
[29] M.S. Daw, M.I. Baskes, Semiempirical, quantum mechanical calculation of hydrogen embrittlement in metals, Phys. Rev. Lett. 50 (1983) 1285–1288, https://doi.org/10.1103/PhysRevLett.50.1285.
[30] M.S. Daw, M.I. Baskes, Embedded-atom method: derivation and application to impurities, surfaces, and other defects in metals, Phys. Rev. B. 29 (1984) 6443–6453, https://doi.org/10.1103/PhysRevB.29.6443.
[31] X. Liu, J.B. Adams, F. Ercolessi, J.A. Moriarty, EAM potential for magnesium from quantum mechanical forces, Model. Simul. Mater. Sci. Eng. 4 (1996) 293, https://doi.org/10.1088/0965-0393/4/3/004.
[32] S. Nosé, A unified formulation of the constant temperature molecular dynamics methods, J. Chem. Phys. 81 (1984) 511–519, https://doi.org/10.1063/1.447334.
[33] W.G. Hoover, Canonical dynamics: equilibrium phase-space distributions, Phys. Rev. A. 31 (1985) 1695–1697, https://doi.org/10.1103/PhysRevA.31.1695.
[34] P. Chen, F. Wang, B. Li, Transitory phase transformations during 10–12 twinning in titanium, Acta Mater. 171 (2019) 65–78, https://doi.org/10.1016/j.actamat.2019.04.002.
[35] B. Li, Y. Shen, Q. An, Structural origin of reversible martensitic transformation and reversible twinning in NiTi shape memory alloy, Acta Mater. 199 (2020) 240–252, https://doi.org/10.1016/j.actamat.2020.08.039.
[36] M.I. Baskes, Modified embedded-atom potentials for cubic materials and impurities, Phys. Rev. B. 46 (1992) 2727–2742, https://doi.org/10.1103/PhysRevB.46.2727.
[37] M.I. Baskes, R.A. Johnson, Modified embedded atom potentials for HCP metals, Model. Simul. Mater. Sci. Eng. 2 (1994) 147, https://doi.org/10.1088/0965-0393/2/1/011.
[38] B. Li, E. Ma, Zonal dislocations mediating {10-11}<10-1-2> twinning in magnesium, Acta Mater. 57 (2009) 1734–1743, https://doi.org/10.1016/j.actamat.2008.12.016.
[39] S.G. Song, G.T. Gray III, Structural interpretation of the nucleation and growth of deformation twins in Zr and Ti—I. Application of the coincidence site lattice (CSL) theory to twinning problems in h.c.p. structures, Acta Metall. Mater. 43 (1995) 2325–2337, https://doi.org/10.1016/0956-7151(94)00433-1.
[40] S.G. Song, G.T. Gray III, Structural interpretation of the nucleation and growth of deformation twins in Zr and Ti—II. Tem study of twin morphology and defect reactions during twinning, Acta Metall. Mater. 43 (1995) 2339–2350, https://doi.org/10.1016/0956-7151(94)00434-X.
[41] X.Y. Zhang, B. Li, J. Tu, Q. Sun, Q. Liu, Non-classical twinning behavior in dynamically deformed cobalt, Materials research letters. (2015) In press.
[42] J.W. Christian, The Theory of Transformations in Metals and Alloys, Newnes, 2002.
[43] M. Niewczas, Lattice correspondence during twinning in hexagonal close-packed crystals, Acta Mater. 58 (2010) 5848–5857, https://doi.org/10.1016/j.actamat.2010.06.059.
[44] B. Li, E. Ma, Atomic shuffling dominated mechanism for deformation twinning in magnesium, Phys. Rev. Lett. 103 (2009), 035503, https://doi.org/10.1103/PhysRevLett.103.035503.
[45] J.A. Yasi, T. Nogaret, D.R. Trinkle, Y. Qi, L.G.H. Jr, W.A. Curtin, Basal and prism dislocation cores in magnesium: comparison of first-principles and embedded-atom-potential methods predictions, Model. Simul. Mater. Sci. Eng. 17 (2009), 055012, https://doi.org/10.1088/0965-0393/17/5/055012.
[46] J.A. Yasi, L.G. Hector Jr., D.R. Trinkle, Prediction of thermal cross-slip stress in magnesium alloys from a geometric interaction model, Acta Mater. 60 (2012) 2350–2358, https://doi.org/10.1016/j.actamat.2012.01.004.
[47] M. Liao, B. Li, M.F. Horstemeyer, Interaction between basal slip and a Mg17Al12 precipitate in magnesium, Metall. Mater. Trans. A. 45 (2014) 3661–3669, https://doi.org/10.1007/s11661-014-2284-3.
[48] B. Zhou, M. Sui, High density stacking faults of $10\bar{1}1$ compression twin in magnesium alloys, J. Mater. Sci. Technol. 35 (2019) 2263–2268, https://doi.org/10.1016/j.jmst.2019.05.042.
[49] H.A. Khater, A. Serra, R.C. Pond, Atomic shearing and shuffling accompanying the motion of twinning disconnections in Zirconium, Philos. Mag. 93 (2013) 1279–1298, https://doi.org/10.1080/14786435.2013.769071.
[50] C.D. Barrett, H. El Kadiri, The roles of grain boundary dislocations and disclinations in the nucleation of 10–12 twinning, Acta Mater. 63 (2014) 1–15, https://doi.org/10.1016/j.actamat.2013.09.012.
[51] B. Li, X.Y. Zhang, Global strain generated by shuffling-dominated twinning, Scr. Mater. 71 (2014) 45–48, https://doi.org/10.1016/j.scriptamat.2013.10.002.
[52] B. Li, X. Zhang, Twinning with zero twinning shear, Scripta Mater. (2016) in press.

[53] B.-Y. Liu, J. Wang, B. Li, L. Lu, X.-Y. Zhang, Z.-W. Shan, J. Li, C.-L. Jia, J. Sun, E. Ma, Twinning-like lattice reorientation without a crystallographic twinning plane, Nat. Commun. 5 (2014), https://doi.org/10.1038/ncomms4297.
[54] B. Li, E. Ma, Li and Ma reply, Phys. Rev. Lett. 104 (2010), 029604, https://doi.org/10.1103/PhysRevLett.104.029604.
[55] B.Q. Li, M.L. Sui, B. Li, E. Ma, S.X. Mao, Reversible twinning in pure aluminum, Phys. Rev. Lett. 102 (2009), 205504, https://doi.org/10.1103/PhysRevLett.102.205504.
[56] J. Towns, T. Cockerill, M. Dahan, I. Foster, K. Gaither, A. Grimshaw, V. Hazlewood, S. Lathrop, D. Lifka, G.D. Peterson, R. Roskies, J.R. Scott, N. Wilkins-Diehr, XSEDE: accelerating scientific discovery, Comput. Sci. Eng. 16 (2014) 62–74, https://doi.org/10.1109/MCSE.2014.80.